Tailoring Dispersion and Interaction of MWNT in Polymer Nanocomposites, Using Triton X-100 as Nonionic Surfactant

Priyanka Pandey, Smita Mohanty, and Sanjay K. Nayak

This study reports an investigation on the effect of non-ionic surfactant (Triton X-100) on the dispersion of multiwalled carbon nanotubes (MWNTs) inside the polymer matrix. Adsorption of triton X-100 to the MWNTs was confirmed through FTIR. A reduced bundling of MWNT fibrils were noticed in Triton X-100 modified MWNTs (Tr-MWNTs). The polymer nanocomposites were prepared via melt blending technique. The optimization of loading ratio of the MWNTs and Tr-MWNTs was carried out on the basis of mechanical properties. Dynamic mechanical analysis exhibited the much uniform dispersion of the Tr-MWNT inside polymer matrix as compared to that of MWNTs. A faster rate of crystallization was noticed in case of MWNT reinforced nanocomposites, however, a strong filler-polymer interaction could be seen in case of Tr-MWNT filled nanocomposites. Optical microscopic analysis exhibited similar effect of MWNT and Tr-MWNT on the spherulite size of the polymer.

1. Introduction

Carbon nanotubes enjoy a preeminent status in the panoply of nanomaterials, due to their tremendous mechanical properties, for a wide range of applications including polymer nanocomposites (Ref 1-5). However, a high aspect ratio of these particles makes them prone to entanglement and bundling leading to the formation of strong van der Waals interaction arising from tube-tube contact, with interaction energy of ca.500 eV/μm (Ref 6). This high interaction energy renders nanotubes dispersion a challenging task. Out of two approaches (i.e., covalent and non-covalent). The noncovalent approach is superior in the sense that it does not alter the π-electron cloud of graphene, and it also does not break the structure of nanotubes (Ref 7), in turn preserving the mechanical properties of carbon nanotubes.

A noncovalent approach involves adsorption of the chemical moieties onto the nanotube surface, either via π-π stacking interaction or through coulomb attraction in the case of charged chemical moieties (Ref 8). In various study the surfactants have been used for surface modification of nanotubes in order to improve its dispersion (Ref 9-11) via improved adhesion between filler and polymer (Ref 12-14), which inturn leads to the improved mechanical performances (Ref 15). To date, a wide variety of surfactants have been investigated for dispersion of carbon nanotubes, such as sodium dodecyl benzene-sulfonate (SDBS) (Ref 16), dodecyltrimethylammonium bromide (DTAB) (Ref 17), hexadecyltrimethylammonium bromide (CTAB) (Ref 18), octyl phenol ethoxylate (Triton X-100) (Ref 19), and sodium dodecyl sulfate (SDS) (Ref 20). Wherein, surfactant Triton X-100 has been found to be efficient in breaking the nanotube aggregates from the recent study (Ref 21).

Till date, most of the researches focused on the surfactants treatment of multiwalled carbon nanotubes (MWNTs), and its effect on breaking nanotube bundles, but paid less attention toward its effect on polymer nanocomposites. In this work, a nonionic surfactant, polyoxyethylene octyl phenyl ether (Triton X-100), has been used to modify the MWCNTs. The study was aimed to investigate the effect of Triton X-100 treated MWNTs (i.e., Tr-MWNTs) on the dispersion of MWNT fibrils into polymer matrix, which is important in achieving the optimum mechanical properties. Polymer nanocomposites reinforced with the MWNTs and Tr-MWNTs were prepared via melt blending technique and optimization of filler/polymer ratio, on the basis of mechanical properties, was carried out. Further the dynamic mechanical properties of nanocomposites were analyzed in order to evaluate the effect of Triton X-100 surfactant on dispersion of carbon nanotubes into polymer matrix. Also the effect of surfactant treated MWNTs on the crystallization properties were analyzed using the Aarami equation.

Further, the experimental trend was correlated with the chemical structure of the surfactants. It was evident that Triton X-100 treated MWNT (Tr-MWNT) enjoys the higher dispersing power by virtue of the benzene ring present in surfactant molecule. Being a mostly utilized thermoplastic material

Priyanka Pandey, Central Institute of Plastics Engineering and Technology (CIPET), T.V.K Industrial Estate, Guindy, Chennai 600032, India; and **Smita Mohanty** and **Sanjay K. Nayak,** Central Institute of Plastics Engineering and Technology (CIPET), T.V.K Industrial Estate, Guindy, Chennai 600032, India and Laboratory for Advanced Research in Polymeric Materials (LARPM), CIPET, Bhubaneswar 751024, India. Contact e-mail: papers.journal@gmail.com.

polypropylene (PP) blend with maleic anhydride grafted PP (MAPP) has been used as the matrix polymer for the preparation of nanocomposites.

2. Experimental

2.1 Triton X-100, Functionalization of MWNTs

A nonionic surfactant, polyoxyethylene octyl phenyl ether (Triton X-100) was used to modify the MWNT surface. In order to treat the MWNTs with Triton X-100, the MWNTs and Triton X-100 were added into the absolute ethanol, at a desired ratio, and then the mixture was subjected to ultrasonication for 1 h. The solution was kept for drying in a vacuum oven at 40 °C for 2 days. During drying process Triton X-100 surfactant is condensed on the surface of MWNTs. A concentration of 1:350 was used in order to achieve the uniform dispersion. Since, the quality of nanotube dispersion deteriorates below or above this ratio (Ref 21). Thus, surfactants should be in concentration just sufficient to coat the nanotube surface, avoiding any excess, as an unnecessarily large amount of surfactant also decreases the nanotube dispersion. The Triton X-100 treated nanotubes are denoted as Tr-MWNT for further discussion.

2.2 Fourier Transform Infra-Red Spectroscopy (FTIR)

For the confirmation of successful modification of MWNT the Fourier transform infra-red spectroscopy (FTIR) was carried out using Thermo scientific FTIR (smart orbit ATR 400-4000 cm^{-1} with microscope).

2.3 Transmission Electron Microscope (TEM)

TEM analysis of the samples was carried using transmission electron microscope (JEOL 1200EX, Japan). TEM imaging was carried out at an accelerating voltage of 100 kV. Images were captured using a charged couple detector (CCD) camera for further analysis using Gatan Digital Micrograph analysis software.

2.4 Fabrication of Nanocomposites

The nanocomposites were prepared via a two-step process. In the first step a blend of PP and MAPP (95:5) was prepared using Haake Rheocord, Batch mixer at a temperature of 190 °C for a blending time of 7 min as obtained from another part of our study. The PP/MAPP (95:5) blend is termed as PPg in the further discussion. In the second step the nanocomposites were

prepared with different loading of MWNT and Tr-MWNT into PPg at a temperature of 180, 185, and 180 °C in front, middle, and rear zone, respectively, using microcompounder, M/s DSM explore Netherlands, (Micro 15) with a mixing time of 20 min. Table 1 represents the composition of the nanocomposites used in the study.

2.5 Mechanical Properties

The Izod impact strength of the PP and its nanocomposites has been evaluated using Tinius Olsen, USA, impactometer as per ASTM D 256. The samples were notched prior to the testing prior to loading with hammer of 2 J. The notch depth was taken as 2.53 mm with a notch angle of 45°. The microinjection molded samples of diameter $63.5 \times 12.7 \times 3$ mm^3 has been used for the testing. Seven numbers of specimens of each composition have been tested in order to get the accuracy in the result.

Further, the microinjection molded dog-bone shaped samples (five specimens of each composition) have been subjected to tensile test. Tensile properties of the virgin matrix as well as the nanocomposites have been evaluated using Universal Tensile Machine (3382 Instron, UK) as per ASTM D 638. Samples of $127 \times 12.7 \times 3$ mm^3 dimension were subjected to tensile test at a gauge length of 50 mm and with cross-head speed of 20 mm/min.

2.6 Dynamic Mechanical Analysis (DMA)

The samples were tested using dynamic mechanical analysis (DMA, TA Instruments Q800) to determine the effects of dispersing agents on the composite samples. The samples were tested at 10-200 °C at 3 °C/min to obtain information across the glass transition temperature. The DMA analysis was conducted in dual cantilever mode at variable temperature using Dynamic mechanical analyzer (DMA Q-800; TA instruments) technique. The experiment was performed on the micro-injection molded samples having a dimension $63.5 \times 12.7 \times 3$ mm^3 was used.

2.7 Differential Scanning Calorimeter (DSC)

Differential scanning calorimetry (DSC) measurement was carried out by scanning the sample about 10 mg, from -50 to 200 °C with heating rate of 10 °C/min under nitrogen atmosphere using Q 20 series of TA instrument. Further, in order to study the crystallization kinetics of the materials all the compositions has been allowed to cool at different crystallization temperature of 117, 118, and 119 °C.

2.8 Optical Microscopic Analysis

The spherulitic morphology of the PP its nanocomposites was investigated using optical microscope DM 4500, Leica Germany. A real-time observation for crystallization process and spherulite growth was performed by using a CCD color camera linked with polarized optical microscope (POM) in constant interval. The samples were sandwiched and melted between two microscope cover slips for observation. The melting of the sample was performed in two steps. First it was heated to 100 °C with a heating rate of 30 °C/min followed by heating to 200 °C with a rate of 20 °C/min in order to erase the thermo-mechanical history. The sample was kept for 5 min at this temperature in order to ensure complete melting. Further to investigate the spherulitic structure the sample was allowed to cool and crystallized at given temperature with a rate of 10 °C/min to a temperature of 150 with an isotherm of 10 min.

Table 1 Compositions for nanocomposites

	Weight % in PPg	
Sample code	MWNT	Tr-MWNT
PPg/MWNT(0.1)	0.1	0
PPg/MWNT(0.3)	0.3	0
PPg/MWNT(0.5)	0.5	0
PPg/Tr-MWNT(0.1)	0	0.1
PPg/Tr-MWNT(0.3)	0	0.3
PPg/Tr-MWNT(0.5)	0	0.5

Further cooling was carried out with lower rate of 3 °C/min to the room temperature. The morphologies were recorded at constant time intervals. The radius of the spherulite was measured and summarized.

3. Materials

PP (M110) was procured from M/s Haldia Petrochemicals, Kolkata, India, having a density of 0.94 g/cm^3 and the MFI of 11 g/10 min. Multiwalled carbon nanotubes of >98% purity and diameter of 80-100 nm, used in this work was purchased from M/s Nanoshel, Intelligent Materials Pvt. Ltd, India. Before using the MWNT for Triton X-100 treatment and incorporation into polymer matrix, the MWNT received, was further purified in presence of HNO$_3$ acid in order to improve the possibility of reactive sites, and it is named as MWNT in the further discussion. The compatibilzer used in this study was MAPP, (OPTIM-P425), having an anhydride content of 1.6-2.5% and density 0.91 g/cm^3 was purchased from M/s Pluss Polymers Pvt. Ltd., Haryana, India.

4. Results and Discussion

4.1 Fourier Transform Infrared Spectroscopy (FTIR)

In order to confirm the adsorption of the Triton X-100, the FTIR analysis of the samples was carried out and represented in Fig. 1. The prominent absorption band at 1574 cm^{-1} was noticed in case of pristine MWNT, this corresponds to the carbon skeleton of the nanotubes. From the spectrum of Tr-MWNT, a broad peak at 3439 cm^{-1} was noticed, which may be due to the OH stretching vibration, exhibiting that some residual terminal hydroxyl groups of surfactant were unreacted. The peaks at 2920 and 2851 cm^{-1} can be assigned to the C-H stretching vibration of -CH$_2$- groups. The band at 1638 cm^{-1}, is due to -C=C- stretch vibration of MWNTs; and 1439 cm^{-1} is due to C-H bending vibration of alkyl chain. The peak at 1274 cm^{-1}, can be assigned to C-O-C stretch vibration. Hence the above mentioned peaks confirm that Triton-X functionality was introduced onto the side walls of MWNTs.

4.2 Transmission Electron Microscope (TEM)

The morphological characterization was carried out using TEM technique and the results are shown in Fig. 2. The CNT samples were dispersed in ethanol for 2 h and dropped on copper grid. TEM micrographs of pristine MNWT exhibited aggregation. However, individual fibers were visible in case of Tr-MWNT. In case of Tr-MWNT the bundling was found to be minimized as compared to MWNT. This may result in the relatively better dispersion of Tr-MWNTs in polymer matrix. Further, no damage in the surface of Tr-MWNTs was noticed after adsorption of Triton X-100 surfactant.

4.3 Mechanical Properties

The mechanical properties of PP nanocomposites reinforced with MWNTs and Tr-MWNTs were evaluated through analyzing their tensile and impact properties. The microinjection molded samples were tested for this purpose. In order to
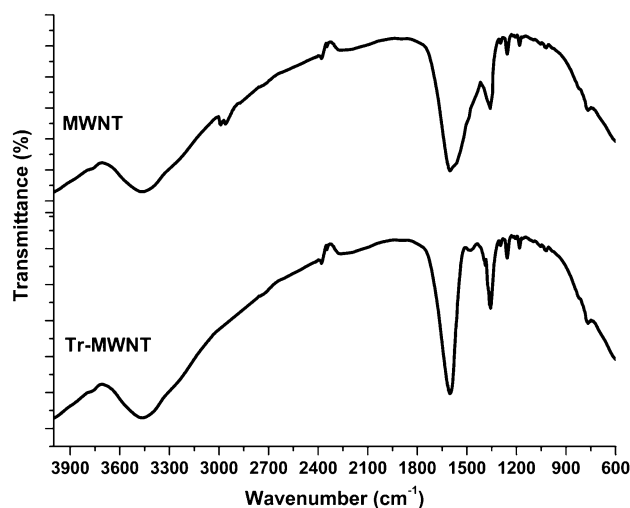

Fig. 1 FTIR spectrum of MWNT and Tr-MWNT

maintain the accuracy of results several samples of each composition were tested.

4.3.1 Investigation of Optimum Filler Concentration. In order to evaluate the optimum concentration of MWNT and Tr-MWNT loading in PPg, the mechanical behavior of nanocomposites reinforced with various loading of MWNTs and Tr-MWNTs was investigated and reported in the Table 2. It is very important to consider that too low filler content would not be able to enhance the properties of PP/MAPP blend (PPg), while addition of too high content of filler may lead to bundling of nanotube fibrils inside the polymer matrix. Therefore it is necessary to investigate the optimum concentration of nanotube loading.

Figure 3 represents the tensile modulus and tensile strength of PP nanocomposites with different loading of MWNTs and Tr-MWNTs. It was evident that both the fillers (i.e., MWNTs and Tr-MWNTs) revealed similar trend of tensile modulus and strength. The modulus of the nanocomposites showed a continuous increase with the increased filler content in both cases (i.e., MWNTs and Tr-MWNTs). Similarly an increasing trend was evident in case of tensile strength of the nanocomposites up to the loading of 0.3% of MWNTs and Tr-MWNTs. Further, increase in the loading of MWNT and Tr-MWNT into the polymer matrix resulted in the deteriorated tensile strength, which is ascribed to the bundling or agglomerates of filler particles due to higher loading. This result was in accordance with the earlier studies (Ref 22, 23). This is ascribed to the agglomerates of MWNT and Tr-MWNT in the polymer matrix. These agglomerates may act as defect sites affecting the tensile deformation of the polymer. Hence, it is worth mentioning that, there are two responsible factors, determining the tensile strength of the polymer; i.e., reinforcement by nanotubes and defects by nanotubes. Reinforcement factor plays major role at low loading of the nanotubes, however, at higher loading the defects factor plays major role. Hence, in both the cases loading of 0.3% of nanotubes has been considered as optimum loading to achieve the advantageous properties.

Hence, the nanocomposites reinforced with 0.3% of MWNTs [PPg/MWNT(0.3)] and 0.3% of Tr-MWNT [PPg/Tr-MWNTs(0.3)] was considered for the further studies as optimized compositions.
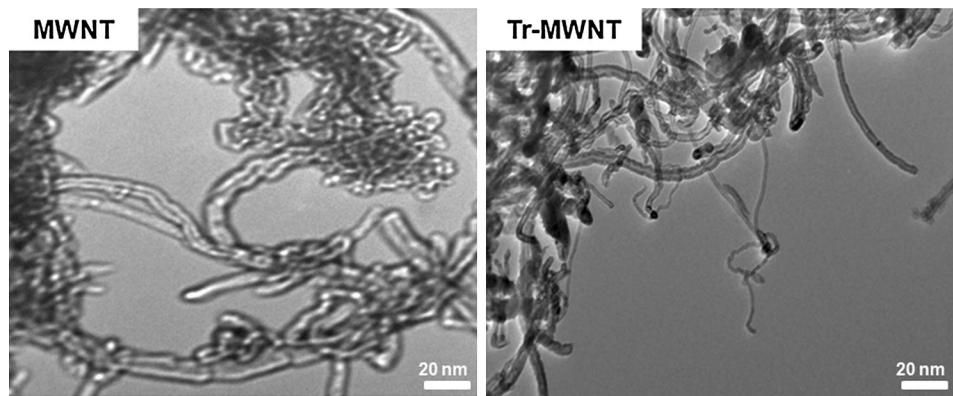
Fig. 2 TEM micrographs of MWNT and Tr-MWNT

Table 2 Mechanical properties of PP and nanocomposites

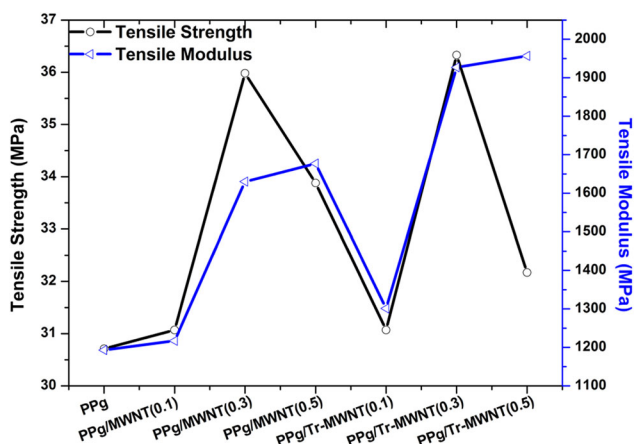| Sample	Yield strength, MPa	Young's modulus, MPa	Elongation at break, %	Impact strength, J/m
PP	30.71 ± 0.18	1193 ± 32	>500	37
PPg/MWNT(0.1)	31.07 ± 0.39	1217 ± 48	>500	38
PPg/MWNT(0.3)	35.98 ± 0.27	1630 ± 60	>500	47
PPg/MWNT(0.5)	33.88 ± 0.39	1677 ± 65	>500	40
PPg/Tr-MWNT(0.1)	31.07 ± 0.39	1301 ± 65	>500	37
PPg/Tr-MWNT(0.3)	36.33 ± 0.41	1727 ± 57	>500	51
PPg/Tr-MWNT(0.5)	32.17 ± 0.39	1711 ± 65	>500	43

Fig. 3 Tensile strength and modulus of PPg and its nanocomposites

4.3.2 Effect of Triton X-100 Adsorbed MWNTs. An increase of 45 and 31% was noticed in the tensile modulus and increase of 10% and 4% in the tensile strength of PPg/Tr-MWNT(0.3) and PPg/MWNT(0.3), respectively, as compared to PPg. Since, both MWNTs and Tr-MWNTs could act as defect sites affecting tensile deformation of a polymer, hence the reason behind the difference between their effects on tensile deformation may be arising from the much improved difference between the dispersion of Tr-MWNT due to relatively strong interfacial interaction with the polymer matrix. Hence, revealing that the efficiency of Triton X-100 to break the nanotube aggregates (Ref 24). This may be attributed to the decreased van der wall forces among MWNTs resulting in its improved dispersion inside polymer matrix.

4.4 Dynamic Mechanical Analysis (DMA)

In order to interpret the unique property variation of PPg and its nanocomposites, including melt fluidity, crystallization habit, thermal stability as well as storage modulus the role of addition of nanofillers on the mobility of polymer chains needs to be identified. The storage modulus is related to the stiffness of the material and measures the elastic response of the polymer. The loss modulus denotes the energy dissipated by the system in the form of heat and measures the viscous response of the polymer material. The damping factor (tan δ) is ratio of loss modulus to storage modulus. Figure 4(a) and (b) represents variation of storage modulus and loss modulus with respect to temperature. In PPg over the entire temperature range; two main mechanical relaxation processes were evident, namely high temp α relaxation, related to the crystalline fraction present and a β process, related to the glass/rubber transition relaxation. It was noticed that α-relaxation in case of nanpo-composites [i.e., PPg/MWNT(0.3) and PPg/Tr-MWNT(0.3)] was shifted toward higher temperature as compared to that of PPg. Further, higher α-relaxation temperature of PPg/Tr-MWNT(0.3) as compared to PPg/MWNT(0.3), exhibited the higher surface area of Tr-MWNT particles in PPg matrix, arising from the relatively finer dispersion of Tr-MWNT inside the PPg matrix (Ref 25). This may be attributed to the ability of the Triton X-100, adsorbed on the surface of MWNTs, to dissociate the bundles or aggregates of the MWNTs into individual one (Ref 24). This further leads to the much easily transferred applied stresses from matrix onto the MWNT particles. Further, it was also noticed, that the curves tend to converge to that of PPg when approaching the melting temperature of PPg. This, convergence, at higher temperature reveals the exploitation of both type of fillers as reinforcement for matrix polymer.

Further, the β relaxation, related with the local motion of amorphous phase, corresponding to t_g of PPg was observed at 17 °C and there was no further, change could be noticed in that of nanocomposites, revealing the equal level of crystallinity of PPg and its nanocomposites. Hence, it is evident that incorporation of MWNT and Tr-MWNT does not alter the relaxation mechanism of macromolecular chains. This may be attributed to the rapid crystallization of polymer and thus the anticipated effect of reinforcement is masked.

Figure 5 represents the damping factor of PPg and nanocomposites. The damping in the polymeric material is sensitive of segmental mobility of the polymer chains and in nanocomposites, is the indicative of interfacial interaction between the polymer and the filler. Strong interfacial interaction between the polymer and the filler tends to restrict the polymer mobility thereby reducing the damping. Wherein, the lowest damping factor of PPg/Tr-MWNT(0.3) as compared to PPg/MWNT(0.3) revealed the relatively strong filler polymer interaction in PPg/Tr-MWNT(0.3), revealing the restricted polymer mobility, arising from the Triton X-100 attached onto the surface of MWNTs which inturn increase the steric hinderance of MWNTs and act as chemical bridging agent of Coulomb interactions.

4.5 Differential Scanning Calorimeter (DSC)

4.5.1 Crystallization Characteristic and Micro-structural Properties. DSC technique is the most convenient method for analyzing the first order transitions like melting and crystallization. Hence to analyze these transitions in PPg and its nanocomposites the samples were subjected to the DSC analysis at a temperature range of −50 to 200 °C with a scanning rate of 10 °C/min. The results obtained are presented in Table 3.

For all cases two cycles were recorded and the thermal characteristics were evaluated always from the second one in order to erase any previous thermal history of sample. Not much significant difference could be noticed in the melting temperature of the PPg and both the nanocomposites. However, a narrower melting peak of both the nanocomposites as compared to neat PPg was evident. Similarly The onset temperature of crystallization $T_{c(onset)}$ and the end crystallization temperature; $T_{c(end)}$ has been shifted toward the higher temperature. Similar to melting, the crystallization peak of both the nanocomposites was found narrower as compared to PPg. Higher thermal conductivity of the

carbon nanotubes, as compared to that of polymer, at least in part may be responsible for the sharper crystallization and melting peak, as heat will be more evenly distributed in the samples containing the carbon nanotubes.

$$X = \frac{\Delta H_m}{f_p \Delta H_m^0} \times 100. \qquad (Eq\ 1)$$

The values of crystallinity obtained using Eq 1 are shown in Table 3. It was noticed that the crystallinity of PPg decreased evidently with incorporation of MWNTs and Tr-MWNTs. The reason for the lower crystallinity of nanocomposites than unfilled PPg can be explained as follows. The filler particles could provide nucleating sites for crystallization of PPg, but at the same time the mobility of polymer chains is restricted by solid filler particles (Ref 26-28). In addition, solid filler particles may also act as barriers affecting crystal growth. As a result, although crystallization of PPg in a nanocomposite could occur earlier at a higher temperature, the amount of polymer crystals formed was limited due to the presence of filler particles. The crystallinity of PPg/MWNT(0.3) composites had the similar trend as the PPg/Tr-MWNTs(0.3) nanocomposites but was much lower than the later one. This can be
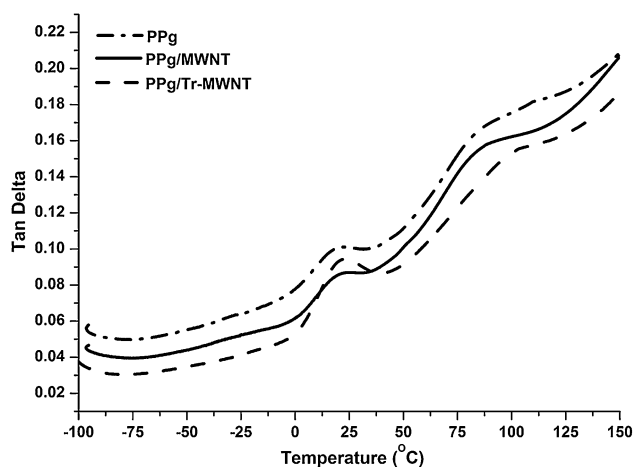

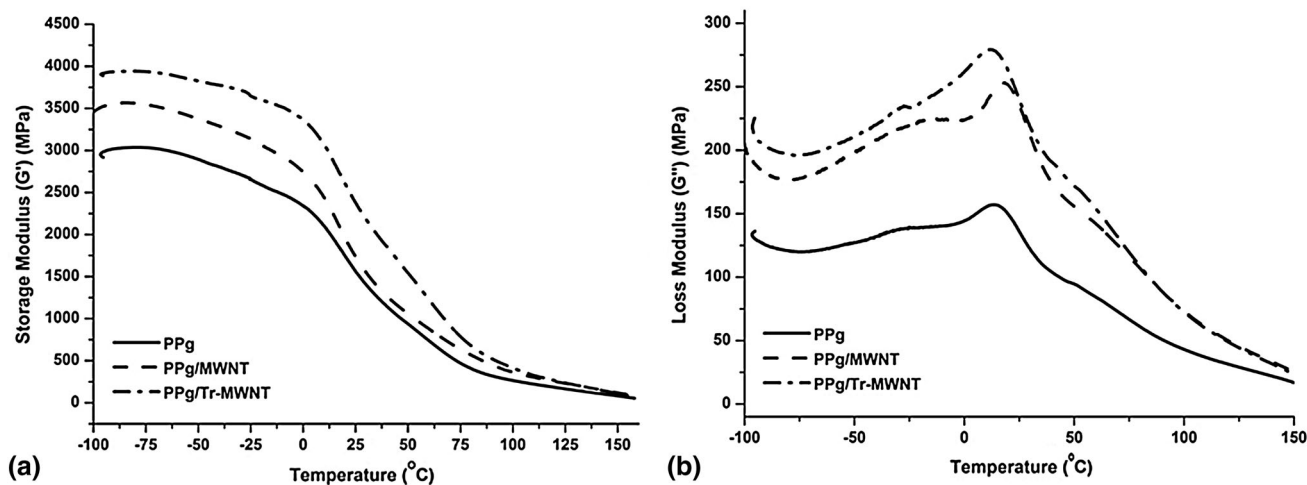**Fig. 5** Tan delta (tan δ) vs. temperature of PPg and its nanocomposites

Fig. 4 (a) Storage modulus vs. temperature. (b) Loss modulus vs. temperature of PPg and its nanocomposites

Table 3 Melting and crystallization temperature of the PP and its nanocomposites

Material	T_m, °C	$T_{c\ (onset)}$, °C	$T_{c\ (end)}$, °C	T_c, °C	Crystallinity, % X_c
PPg	175.5	119.3	110.2	88.1	64
PPg/MWNT(0.3)	169.45	123.8	118.7	96.3	62.2
PPg/Tr-MWNT(0.3)	169.66	127.1	120	103.9	57.1
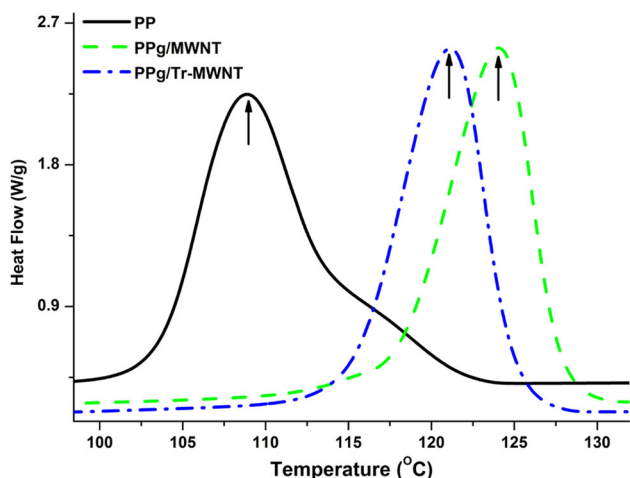
Fig. 6 DSC thermogram of PPg and its nanocomposites

explained by the stronger interaction at the Tr-MWNTs and polymer, interface which attracts some polymer chains in the vicinity of Tr-MWNTs from crystallization. As a result, the PPg in the presence of Tr-MWNT could not crystallize as much as it in the presence of MWCNTs.

Figure 6 shows the crystallization curves for the PPg/MWNT(0.3) and PPg/Tr-MWNT(0.3) nanocomposites on cooling. In all the cases there was only one single exothermic peak appearing between 133 and 100 °C, which was identified as the crystallization peak, and the peak temperature of the exothermic peak was defined as its crystallization temperature (T_c). The crystallization temperature of unfilled PPg is 108 °C. From Fig. 6, it is interesting to note that the addition of both fillers (i.e., MWNTs and Tr-MWNTs) could shift the crystallization temperature of PPg to higher extent. The higher crystallization temperatures of nanocomposites as compared to that of PPg meant that crystallization started earlier in the nanocomposites than in the PPg. This is because the fillers could act as nucleating agents to induce crystallization of the polymer melt in the cooling process. The effect of fillers on T_c is found to be different in such an order: MWNTs > Tr-MWNTs. This result suggests that MWCNTs were a more effective nucleating agent for matrix polymer than Tr-MWNTs. The difference in affecting T_c between MWCNTs and Tr-MWNTs is considered to be due to the stronger interfacial interaction between Tr-MWNTs and polymer in the PPg/Tr-MWNT nanocomposites than that between MWCNTs and PPg in the PPg/Tr-MWNTs nanocomposites. The stronger interaction at the Tr-MWNTs interface would tend to 'attract' polymer chains from crystallization. As a result, the PPg in the presence of Tr-MWNTs could not crystallize as early as it in the presence of MWNTs. This was in accordance with the earlier findings about nucleating effect of MWNTs (Ref 29-32).

4.5.2 Isothermal Crystallization Kinetics. In order to investigate the nucleating effect of both MWNT and Tr-MWNT more accurately, the crystallization kinetics study of the materials has been carried out. The analysis was performed according to the Avrami theory represented by Eq 2. By using the Avrami equation, the crystallization kinetics of polymers can be well approximated under isothermal condition for various modes of nucleation and growth.

$$X_t = 1 - \exp[-Kt^r]. \tag{Eq 2}$$

K is the crystallization rate constant/kinetic growth rate constant; X_t is crystalline conversion at time t; r is the Avrami exponent, which is a constant depending on the mechanism of nucleation, form of crystal growth as well as geometry of the growing crystals (Ref 33).

Avrami exponent r can be calculated using Eq 3.

$$r = 1/[1 + \ln(n) - \ln(n + m)]. \tag{Eq 3}$$

Value of n and m can be obtained from the DSC run using the TA software. Figure 7 represents the plots of [log ($-\ln$ $(1 - X_t)$] versus log t for all the materials studied, at different isothermal temperatures. The analysis revealed good linearity of [log ($-\ln$ $(1 - X_t)$] versus log t curve in wide relative crystalline range at different temperature. Hence, the crystallization process was well described by Avrami equation as can be seen by the good fit between the linear regression and the experimental data. According to the nucleation and growth mechanism the Avrami exponent r should be an integer value. However, the value found through DSC experiment was ranging from 2.9 to 3.7 (not an integer). For PPg the value of r (Avrami exponent) was obtained as 2.9, over the crystallization temperature range studied. This was in accordance with the previous studies (Ref 34). For PPg/MWNT and PPg/Tr-MWNT the Avrami exponent was obtained as 3.3 and 3.7, respectively.

The values of Avrami exponent of PPg exhibited the homogenous nucleation with two dimensional growths. However, from the increase in the value of r for nanocomposites, change from two dimensional to three dimensional crystals growth of polymer matrix was evident. Therefore, it was assumed that the crystallization of matrix polymer is controlled by homogenous nucleation, whereas the nucleation mechanism was modified in the nanocomposites. This modification might be attributed to higher crystallization rate. The higher crystallization rate of nanocomposites was ascribed to reduced average activation energy which might be a result of preexisting nuclei in polymer matrix, introduced due to presence of heterogeneities (i.e., fillers) in nanocomposites (Ref 34).

Figure 8(a) represents crystallization half time ($t_{1/2}$) obtained from the isothermal crystallization curves of PPg and its nanocomposites. This is time corresponding to the time necessary for a polymer to reach 50% of its maximum crystallinity. However, the $t_{1/2}$ for the nanocomposites was lower than that of PPg revealing the increased crystallization rate of PPg due to incorporation of MWNTs and Tr-MWNTs.
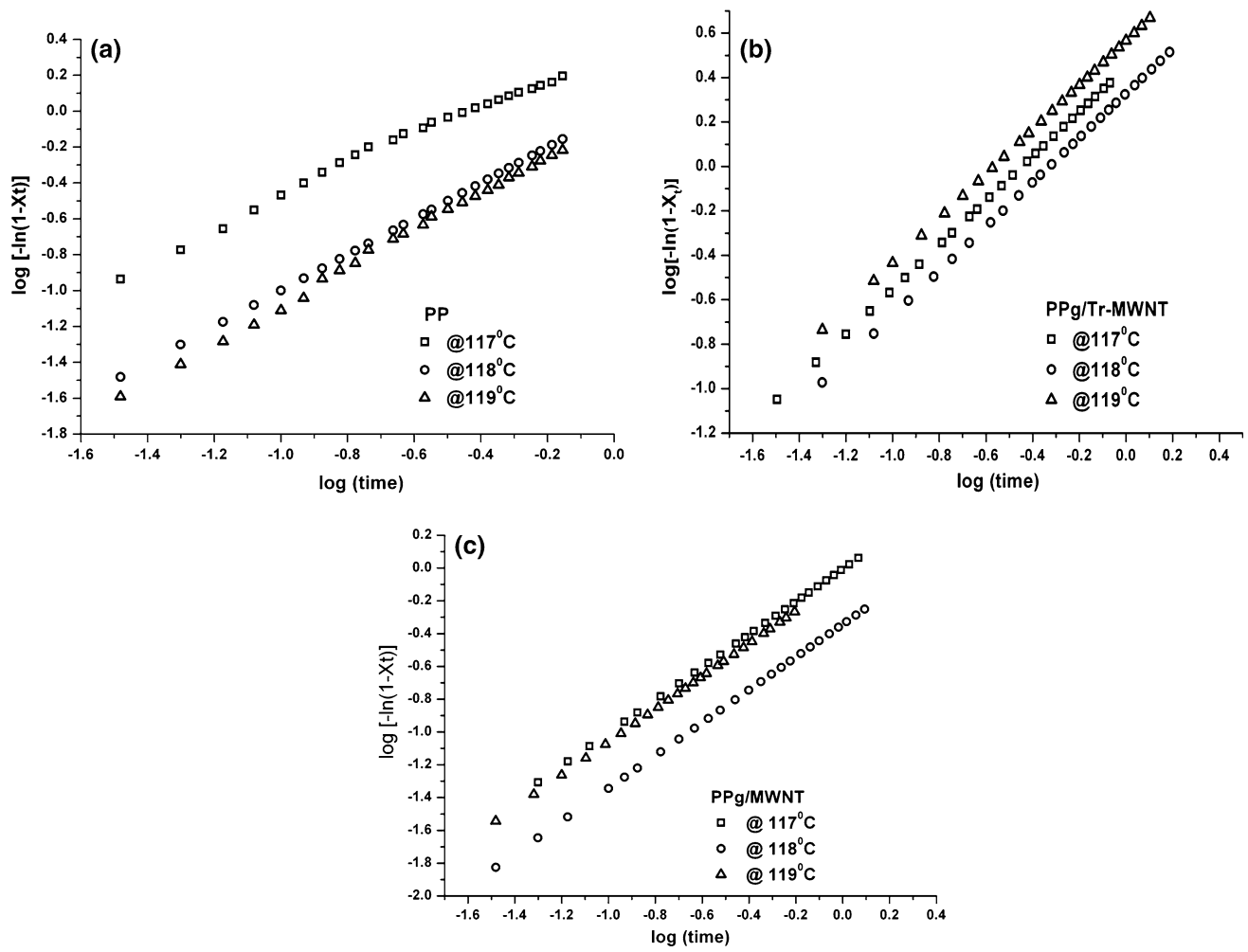
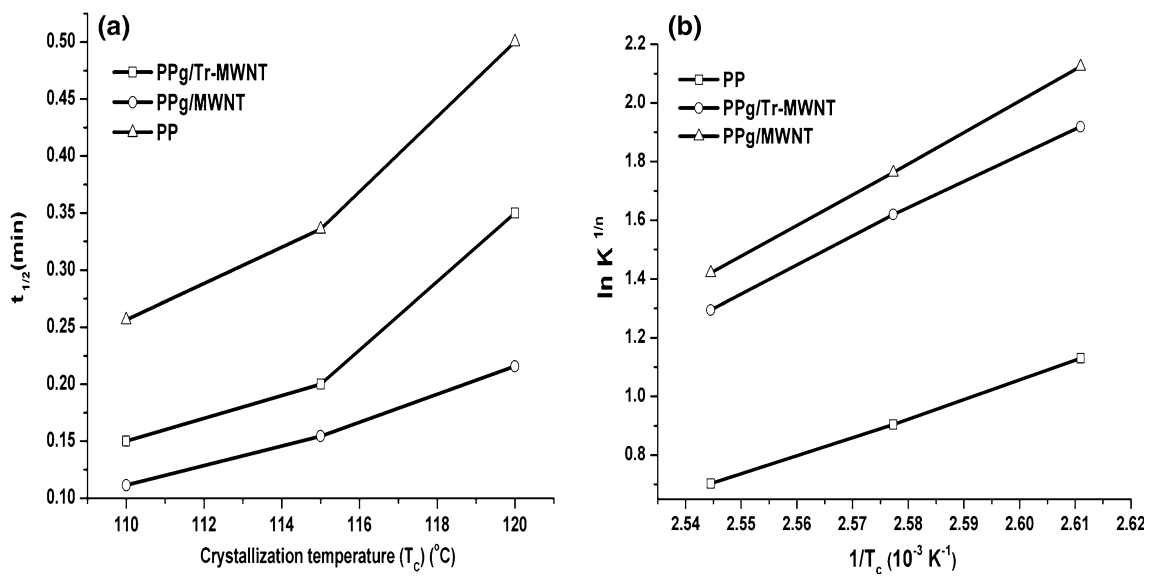Fig. 7 Avrami plot at selected temperatures of PPg and nanocomposites

Fig. 8 (a) Half life time ($t_{1/2}$) vs. crystallization temperature. (b) ln $K^{1/n}$ vs. $1/T_c$ of PPg and its nanocomposites

This might be attributed to the nucleation effect of fillers on the crystallization of PPg. However, the lower $t_{1/2}$ value of PPg/MWNT(0.3) as compared to PPg/Tr-MWNT(0.3), was in accordance with the previous observation, exhibiting the stronger interaction at the Tr-MWNT/PPg interface, resulting into 'attraction' of polymer chains from crystallization, which subsequently leads to delayed completion of crystallization process in PPg/Tr-MWNT(0.3) as compared to PPg/MWNT(0.3). The crystallization rate constant of the materials was estimated according to Eq 3. The faster crystallization of PPg/MWNT(0.3) as compared to PPg/Tr-MWNT(0.3) was further confirmed by the lower value of crystallization constant value (K) of PPg/MWNT(0.3) as shown in Fig. 8(b).

$$K^{\frac{1}{n}} = A \exp\left(-\frac{\Delta E}{RT}\right). \qquad \text{(Eq 4)}$$

The values of activation energy, ΔE, can be obtained from the slope of linear fitting of the plot $\ln K^{1/n}$ versus $1/T_c$, using Eq 4, as represented in Fig. 8(b). The activation energy for both the nanocomposites has been found lower revealing the slower diffusion of polymer chains in tortuous path due to good dispersion of filler particles in polymer matrix. Wherein the lowest activation energy of the PPg/MWNT(0.3) exhibited relatively high nucleating effect of MWNTs as compared to Tr-MWNTs.
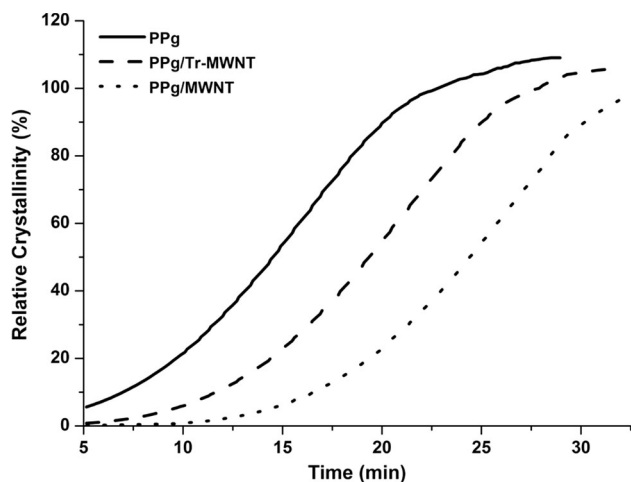

Fig. 9 Relative crystallinity of PPg and its nanocomposites at 118 °C T_c

Since, the crystallinity plays a major role in deciding the properties of polymer. In order to compare the crystallinity of the PPg and its nanocomposites, the curve between relative crystallinity versus time was analyzed. However, from the relative crystallinity curve similar sigmoidal shape, as represented in Fig. 9, has been observed for PPg and both nanocomposites. It was evident that the curve for nanocomposites was shifted to the right, revealing the higher crystallization rate of nanocomposites. Wherein the curve of PPg/MWNT(0.3), right to the PPg/Tr-MWNT(0.3) showed the higher crystallization rate of previous one. Hence, from the crystallization, studies it was evident that the nucleating effect of MWNT is higher than that of Tr-MWNTs, however, a much strong interaction between filler and polymer could be achieved via modification of MWNTs using Triton X-100.

4.6 Optical Microscopic Analysis

Figure 10, represents optical microscopic images of PPg and its nanocomposites. PPg exhibits four leaf clover patterns when it is crystallized. The presence of four leaf clover pattern exhibited high ordering of tangential and radial lamellae in spherulites. The spherulitic size of PPg was found approximately 152 μm in diameter. The Mattese cross pattern could be observed in the spherulitic growth.

Unlike to PPg, its nanocomposites exhibited smeared four leaf clover pattern. In nanocomposites, less ordered spherulites with rodlike scattering pattern was observed. The rodlike scattering pattern was ascribed to the arrangement of radiating primary lamellae. The spherulitic size of the PPg was found to be higher than that of nanocomposites. Further, it was noticed that the formation of spherulites during cooling has started little earlier in case of PPg/MWNT(0.3) as compared to that of PPg/Tr-MWNT(0.3). However, not much difference in the size of the spherulites was noticed in the case of both the nanocomposites, revealing the similar effect on the spherulitic size.

5. Conclusion

In summary, the nanocomposites Tr-MWNT reinforced PPg have been successfully prepared Triton X-100 as a dispersing aid. It was also evident that Triton X-100 was able to significantly minimize the bundling of the MWNT fibrils, leading to the much uniform dispersion of MWNT. Both pristine MWNTs and Tr-MWNTs could improve tensile modulus and strength, but the Tr-MWNTs had a better effect than MWCNTs due to the fact that Triton X-100 could help
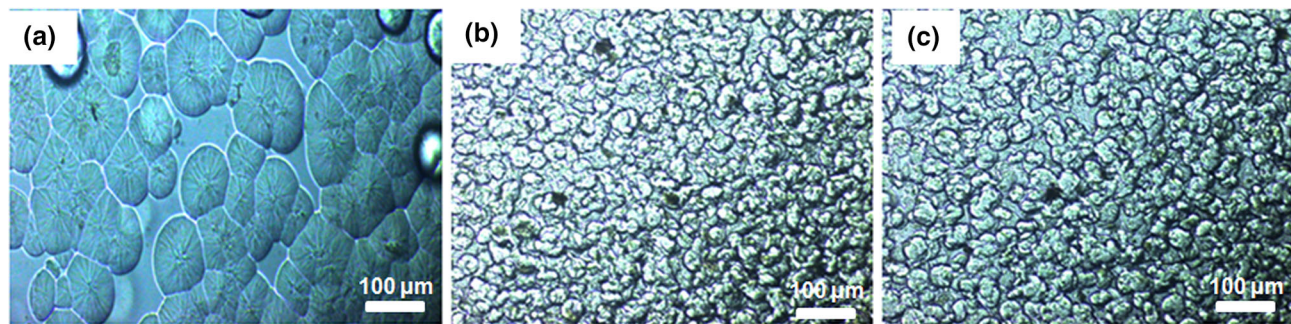

Fig. 10 Spherulitic structure of (a) PPg, (b) PPg/Tr-MWNT(0.3), (c) PPg/MWNT(0.3)

improving the dispersion of MWCNTs by reducing the surface energy and van der Waals forces between MWCNTs. The DMA analysis was further in accordance with the tensile properties, exhibiting the much uniformly distributed stress onto the Tr-MWNT as compared to that of MWNT, resulting in improved stiffness of PPg/Tr-MWNT(0.3). The DSC results confirmed that both pristine MWNTs and Tr-MWNTs acted as nucleating agents in the PP matrix and promoted the nucleation for crystallization of PPg. However, as compared with the PPg/MWNT composites, PPg/Tr-MWNT nanocomposites had lower T_c and X_c because Triton X-100 adsorption had enhanced the interaction at the nanotube-PPg interface. However, no remarkable effect of Triton adsorption onto MWNT, over the spherulite size could be seen. Hence, this study confirmed that Triton X-100 can be efficiently used to enhance the degree of dispersion of the MWNT into the polymer matrix in order to achieve the maximum advantage of the MWNT nanofillers over the mechanical properties of the nanocomposites. Which is achieved due to improved interaction between Triton X-100 treated MWNT and polymer matrix.

References

1. X. Tang, S. Bansaruntip, N. Nakayama, Y. Erhan, Y.L. Chang, and Q. Wang, Carbon Nanotube DNA Sensor and Sensing Mechanism, *Nano Lett.*, 2006, **6**(8), p 1632–1636 (in English)

2. L. Clayton, T. Gerasimov, M. Meyyappan, and J.P. Harmon, Transparent PMMA/SWNT Composites with Increased Dielectric Constants, *Adv. Funct. Mater.*, 2005, **15**(1), p 101–106 (in English)

3. J. Koohsorkhi, Y. Abdi, S. Mohajerzadeh, H. Hosseinzadegan, Y. Komijani, and E.A. Soleimani, Fabrication of Self-defined Gated Field Emission Devices on Silicon Substrates Using PECVD-Grown Carbon Nano-tubes, *Carbon*, 2006, **44**(13), p 2797–2803 (in English)

4. E. Frackowiak and F. Beguin, Electrochemical Storage of Energy in Carbon Nanotubes and Nanostructured Carbon, *Carbon*, 2002, **40**, p 1775–1787 (in English)

5. H.J. Dai, J.H. Hafner, A.G. Rinzler, D.T. Colbert, and R.E. Smalley, Nanotubes as Nanoprobes in Scanning Probe Microscopy, *Nature*, 1996, **384**(6605), p 147–150 (in English)

6. M. Terrones, Science and Technology of the Twenty-First Century: Synthesis, Properties, and Applications of Carbon Nanotubes, *Annu. Rev. Mater. Res.*, 2003, **33**, p 419–501 (in English)

7. H. Oh, B.M. Jung, H.P. Lee, and J.Y. Chang, Dispersion of Single Walled Carbon Nanotubes in Organogels by Incorporation into Organogel Fibers, *J. Colloid Interface Sci.*, 2010, **352**(1), p 121–127 (in English)

8. L.A. Girifalco, M. Hodak, and R.S. Lee, Carbon Nanotubes, Buckyballs, Ropes, and a Universal Graphitic Potential, *Phys. Rev. B*, 2000, **62**(19), p 13104–13110 (in English)

9. N.A. Cordero and J.A. Alonso, Interaction of Surfactants Containing a Sulfuric Group with a (5,5) Carbon Nanotube, *J. Phys. Chem. C*, 2010, **114**, p 17249–17256 (in English)

10. H. Xu, H. Abe, M. Naito, Y. Fukumori, H. Ichikawa, S. Endoh, and K. Hata, Efficient Dispersing and Shortening of Super-Growth Carbon Nanotubes by Ultrasonic Treatment with Ceramic Balls and Surfactants, *Adv. Powder Technol.*, 2010, **21**, p 551–555 (in English)

11. E.J.F. Carvalho and M.C. Dos Santos, Role of Surfactants in Carbon Nanotubes Density Gradient Separation, *ACS Nano*, 2010, **4**, p 765–770 (in English)

12. J. Rausch, R.C. Zhuang, and E. Mäder, Surfactant Assisted Processing of Carbon Nanotube/Polypropylene Composites: Impact of Surfactants on the Matrix Polymer, *J. Appl. Polym. Sci.*, 2010, **117**, p 2583–2590 (in English)

13. Y. Bai, D. Lin, F. Wu, Z. Wang, and B. Xing, Adsorption of Triton X-Series Surfactants and Its Role in Stabilizing Multi-walled Carbon Nanotube Suspensions, *Chemosphere*, 2010, **79**, p 362–367 (in English)

14. J.G. Park, J. Smithyman, C.Y. Lin, A. Cooke, A.W. Kismarahardja, S. Li, R. Liang, J.S. Brooks, C. Zhang, and B. Wang, Effects of Surfactants and Alignment on the Physical Properties of Single-Walled Carbon Nanotube Buckypaper, *J. Appl. Phys.*, 2009, **106**, p 104310 (in English)

15. P. Angelikopoulos and H. Bock, Directed Self-assembly of Surfactants in Carbon Nanotube Materials, *J. Phys. Chem. B*, 2008, **112**, p 13793–13801 (in English)

16. M.F. Islam, E. Rojas, D.M. Bergey, A.T. Johnson, and A.G. Yodh, High Weight Fraction Surfactant Solubilization of Single-Wall Carbon Nanotubes in Water, *Nano Lett.*, 2003, **3**(2), p 269–273 (in English)

17. E.A. Whitsitt and A.R. Barron, Silica Coated Single Walled Carbon Nanotubes, *Nano Lett.*, 2003, **3**(6), p 775–778 (in English)

18. A.G. Ryabenko, T.V. Dorofeeva, and G.I. Zvereva, UV-VIS-NIR Spectroscopy Study of Sensitivity of Single-Wall Carbon Nanotubes to Chemical Processing and Van-der-Waals SWNT/SWNT Interaction. Verification of the SWNT Content Measurements by Absorption Spectroscopy, *Carbon*, 2004, **42**(8-9), p 1523–1535 (in English)

19. H. Wang, W. Zhou, D.L. Ho, K.I. Winey, J.E. Fischer, C.J. Glinka, and E.K. Hobbie, Dispersing Single-Wall Carbon Nanotubes with Surfactants: A Small Angle Neutron Scattering Study, *Nano Lett.*, 2004, **4**, p 1789–1793 (in English)

20. J. Yu, N. Grossiord, C.E. Koning, and J. Loos, Controlling the Dispersion of Multi-walled Carbon Nanotubes in Aqueous Surfactant Solution, *Carbon*, 2007, **45**, p 618–623 (in English)

21. R. Rastogi, R. Kaushal, S.K. Tripathi, A.L. Sharma, I. Kaur, and L.M. Bharadwaj, Comparative Study of Carbon Nanotube Dispersion Using Surfactants, *J Colloid Interface Sci.*, 2008, **328**, p 421–428 (in English)

22. P. Liu, Modifications of Carbon Nanotubes with Polymers, *Eur. Polym. J.*, 2005, **41**, p 2693–2703 (in English)

23. A.A. Koval'chuk, V.G. Shevchenko, A.N. Shchegolikhin, P.M. Nedorezova, A.N. Klyamkina, and A.M. Aladyshev, Effect of Carbon Nanotube Functionalization on the Structural and Mechanical Properties of Polypropylene/MWCNT Composites, *Macromolecules*, 2008, **41**, p 7536–7542 (in English)

24. F. Xin and L. Li, Effect of Triton X-100 on MWNT/PP Composites, *J. Thermoplast. Compos. Mater.*, 2011, **26**(2), p 227–242 (in English)

25. V. Vladimirov, C. Betchev, A. Vassiliou, G. Papageorgiou, and D. Bikiaris, Dynamic Mechanical and Morphological Studies of Isotactic Polypropylene/Fumed Silica Nanocomposites with Enhanced Gas Barrier Properties, *Compos. Sci. Technol.*, 2006, **66**, p 2935–2944 (in English)

26. H. Tsuji, Y. Kawashima, H. Takikawa, and S. Tanaka, Poly(L-lactide)/Nano-structured Carbon Composites: Conductivity, Thermal Properties, Crystallization, and Biodegradation, *Polymer*, 2007, **48**, p 4213–4225 (in English)

27. Q. Duan, B. Wang, B. Hong, and H. Wang, Studies on the Nonisothermal Crystallization Behaviour of Polypropylene/Multi-walled Carbon Nanotubes Nanocomposites, *J. Macromol. Sci. B*, 2010, **49**, p 1094–1104 (in English)

28. A.R. Bhattacharyya, T.V. SreeKumar, T. Liu, S. Kumar, S. Ericson, and R.H. Hauge, Crystallization and Orientation Studies in Polypropylene/Single Wall Carbon Nanotube Composite, *Polymer*, 2003, **44**, p 2373–2377 (in English)

29. O. Probst, E.M. Moore, D.E. Resasco, and B.P. Grady, Nucleation of Polyvinyl Alcohol Crystallization by Single-Walled Carbon Nanotubes, *Polymer*, 2004, **45**, p 4437–4443 (in English)

30. S. Yang, J.R. Castilleja, E.V. Barrera, and K. Lozano, Thermal Analysis of an Acrylonitrile-Butadiene-Styrene/SWNT Composite, *Polym. Degrad. Stabil.*, 2004, **83**, p 383–388 (in English)

31. K.P. Ryan, S.M. Lispon, A. Drury, M. Cadek, M. Ruether, and S.M. Oflaherty, Carbon-Nanotube Nucleated Crystallinity in a Conjugated Polymer Based Composite, *Chem. Phys. Lett.*, 2004, **391**, p 329–333

32. A.K. Anoop, U.S. Agarwal, and R. Joseph, Carbon Nanotubes Induced Crystallization of Poly(ethylene terephthalate), *Polymer*, 2006, **47**, p 3976–3980 (in English)

33. H.N. Beck, Heterogeneous Nucleating Agents for Crystallization of Vinylidene Chloride-Vinyl Chloride Copolymers, *J Appl. Polym. Sci.*, 1975, **19**(2), p 371–373 (in English)

34. R. Nowacki, B. Monasse, E. Piorkowska, A. Galeski, and J.M. Haudin, Spherulite Nucleation in Isotactic Polypropylene Based Nanocomposites with Montmorillonite Under Shear, *Polymer*, 2004, **45**(14), p 4877–4892 (in English)